Continuous Repetitive Data Acquisition with ^{123}I-FP-CIT SPECT: Effects of Rotation Speed and Rotation Time

Norikazu Matsutomo[1], Eri Takano[2], Tomoaki Yamamoto[1], and Eisuke Sato[1]

[1]Department of Medical Radiological Technology, Faculty of Health Sciences, Kyorin University, Tokyo, Japan; and [2]Department of Radiology, Saku Central Hospital, Nagano, Japan

The aim of this study was to evaluate the effects of the acquisition rotation speed and the rotation time for continuous repetitive rotation acquisition (CRRA) on image quality and quantification in ^{123}I-FP-CIT SPECT. **Methods:** An anthropomorphic striatal phantom filled with ^{123}I solution was acquired with CRRA and the step-and-shoot (SS) mode. The following combinations of acquisition rotation speed and rotation time for CRRA were used: 0.50 rpm by 30 frames, 0.17 rpm by 10 frames, 0.10 rpm by 6 frames, and 0.05 rpm by 3 frames. SPECT images were reconstructed using ordered-subset expectation maximization with resolution recovery, scatter, and CT-based attenuation correction. Two kinds of image processing patterns—image reconstruction after the addition of projection data (the added-projection-data process) and image addition after data reconstruction (the added-reconstructed-image process)—were investigated in this study. The effects of the acquisition parameters and the image processes were evaluated by the full width at half maximum, percentage coefficient of variation (%CV), and specific binding ratio (SBR). **Results:** With full width at half maximum, there were no clear differences between CRRA images obtained with the various rotation speeds before rotation and the SS mode. Although the combination of a slow rotation speed and a short rotation time improved image uniformity compared with the SS mode, the %CV obtained by CRRA increased as the rotation speed increased. The %CVs were 11.9% ± 0.9% for 0.50 rpm by 30 frames, 6.9% ± 0.9% for 0.05 rpm by 3 frames, and 9.6% ± 0.5% for SS mode. SBRs obtained by CRRA with the added-projection-data process were equal to those obtained by SS mode. However, SBRs obtained with the added-reconstructed-image process were clearly decreased compared with the SS mode. **Conclusion:** The combination of rotation speed and rotation times affects the image quality and quantification of ^{123}I-FP-CIT SPECT using CRRA. When CRRA is applied in ^{123}I-FP-CIT SPECT, it is necessary to use added-projection-data processes and proper rotation speeds (e.g., 0.10–0.17 rpm rotation speed).

Key Words: continuous repetitive rotation acquisition; dynamic SPECT; step-and-shoot; SPECT; ^{123}I-FP-CIT

J Nucl Med Technol 2019; 47:319–325
DOI: 10.2967/jnmt.119.228783

Dopamine transporter SPECT using ^{123}I-*N*-ω-fluoropropyl-2β-carbomethoxy-3β-(4-iodophenyl)nortropane (^{123}I-FP-CIT) has been widely used for diagnosis and follow-up of Parkinson disease and dementia with Lewy bodies (*1–6*). For image acquisition, guidelines and the Quantitative Imaging Biomarkers Alliance on dopamine transporter SPECT have typically recommended the use of step-and-shoot (SS)–mode acquisition (*7–9*). Alternatively, continuous-mode acquisition can be used to shorten the total scan time. The continuous mode has higher sensitivity than the SS mode because events are acquired during the entire camera rotation. Also, it can reduce the system dead time. In particular, a continuous repetitive rotation acquisition (CRRA) as dynamic SPECT can be performed to better assess tracer clearance and patient motion (*10–12*). Patient motion is often included in the acquisition data because it is difficult for patients with Parkinson disease to keep their head within the head holder without causing them stress. With dynamic SPECT, if significant motion is included in the acquisition frames, these frames are specifically excluded from the image reconstruction process. In addition, for CRRA, because the projection data are completely acquired in a rotation time, SPECT images can be generated (although image quality will be affected) even if an examination has not been completed still. Therefore, a dynamic SPECT acquisition may be useful for dopamine transporter SPECT. However, acquisition parameters such as rotation speed and rotation time have not yet been sufficiently investigated.

In dynamic SPECT acquisitions, the final projection data for image reconstruction are created by the addition of each acquisition frame at the same angle. Because the detected counts in SPECT are independently Poisson-distributed, the noise level does not have a linear relationship to the acquisition time. Therefore, even if the total acquisition time is equal, the reconstructed image quality may be affected by the combination of the rotation speed and the rotation time (e.g., 0.50 rpm by 30 frames or 0.10 rpm by 6 frames). Thus, the purpose of this study was to validate the effects of rotation speed and rotation time for continuous repetitive data acquisition with ^{123}I-FP-CIT SPECT. Using an anthropomorphic striatal phantom, we evaluated the image quality and quantification results of ^{123}I-FP-CIT SPECT obtained

Received Mar. 16, 2019; revision accepted May 13, 2019.
For correspondence or reprints contact: Norikazu Matsutomo, Department of Medical Radiological Technology, Faculty of Health Sciences, Kyorin University, A-420, 5-4-1 Shimorenjaku Mitaka-shi, Tokyo 181-8612, Japan.
E-mail: nmatsutomo@ks.kyorin-u.ac.jp
Published online Jun. 10, 2019.

with several combinations of acquisition rotation speed and rotation time.

MATERIALS AND METHODS

SPECT/CT Instrument and Phantoms

All experimental data were acquired with a dual-head SPECT/CT camera (Infinia 8 Hawkeye 4; GE Healthcare) equipped with a low-energy, high-resolution collimator. This system has 2.54-cm (1-in) crystals and a spatial resolution of 8.1 mm at 140.5 keV and 10 cm from the collimator. The CT component was a low-dose multislice CT system. For the analysis, we used a striatal phantom (NMP Business Support Co., Ltd.). The striatum and background of the phantom were filled with ^{123}I solution (^{123}I-FP-CIT) that had an approximately 8:4:1 radioactivity ratio (right striatum, 61.4 kBq/mL; left striatum, 30.7 kBq/mL; background, 7.9 kBq/mL).

Date Acquisition

All projection data were obtained in continuous repetitive data acquisition mode with rotation through 60 projections per head and a circular orbit of 360°. The pixel size was 2.95 mm with a 128 × 128 matrix (scale for enlargement, 1.5), and the radius of rotation was set at 14 cm. A photopeak of ^{123}I was set as a 20% energy window centered at 159 keV. A subwindow to correct the dual-energy window scatter was set at a 10% energy window centered at 130 keV. Total acquisition time was 30 min, with several rotation speeds and several rotation times in the following combinations: 0.50 rpm by 30 frames, 0.17 rpm by 10 frames, 0.10 rpm by 6 frames, and 0.05 rpm by 3 frames. A SPECT image obtained in SS mode (3° arc per step and 30 s/view) was defined as the reference image. A low-dose CT scan was performed using the following parameters: 120 kV, 2.5 mA, and 1.9 pitch.

Image Reconstruction

All SPECT images were reconstructed using ordered-subset expectation maximization with resolution recovery, scatter, and CT-based attenuation correction. The reconstruction parameters were 10 subsets and 2 iterations. The images were reconstructed by postprocessing with a Butterworth filter (cutoff frequency, 0.48 cycles/cm; power factor, 10), and a dual-energy window was used for scatter correction. Two image processing patterns were compared in this study (Fig. 1). The first approach involved image reconstruction with the addition of projection data (the added-projection-data process). The second approach involved image addition after data reconstruction (the added-reconstructed-image process).

Data Analysis

To investigate the effect of acquisition parameters, the effective spatial resolution and percentage coefficient of variation (%CV) were calculated. Effective spatial resolution was evaluated by the full width at half maximum (FWHM) at the striatum (Fig. 2A). For calculation of FWHM, a capillary point source phantom would be preferred. However, we used the anthropomorphic striatal phantom because the aim was to evaluate the effective spatial resolution in ^{123}I-FP-CIT images. In addition, we placed the elliptic background volume of interest (VOI) with a 25 cm^3 area on the occipital region of the phantom (Fig. 2B). The %CVs of the background were calculated as follows:

$$\%\mathrm{CV} = \frac{\mathrm{SD}_b}{C_b} \times 100\%,$$

where C_b is the mean count in the background VOI and SD_b is the SD of the background area based on the variance in individual voxels within the VOI. We assessed the quantitative index accuracy by measuring the specific binding ratio (SBR) on the phantom images. For the SBR calculation, we used DaTView (AZE), developed on the basis of the Southampton method (*13*). This method is a semiautomated analysis with 3 features: manual placement of the whole striatal VOI, automated creation of the reference VOI, and calculation of the SBR. First, the whole striatal VOI was set on the summed images oriented in the orbitomeatal plane. Second, the reference VOI for the estimation of the nonspecific count was set on the whole brain with exclusion of the striatum. Finally, the SBR was calculated as follows:

$$\mathrm{SBR} = \frac{\frac{Ct_{\mathrm{VOI}}}{C_r} - V_{\mathrm{VOI}}}{V_s},$$

where V_s is the standard volume of the striatum (11.2 mL), Ct_{VOI} is the total count in the striatal VOI, C_r is the count concentration in the reference VOI, and V_{VOI} is the volume of the striatal VOI.

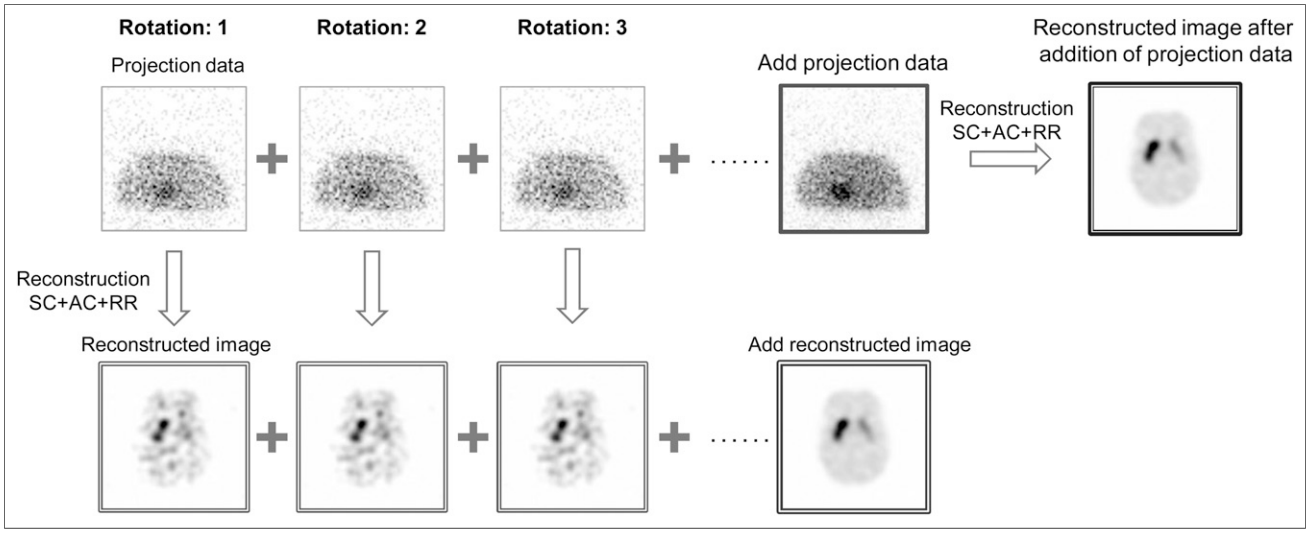

FIGURE 1. Image reconstruction from acquisition data by added-projection-data process and by added-reconstructed-image process. SC = scatter correction; AC = attenuation correction; RR = resolution recovery.

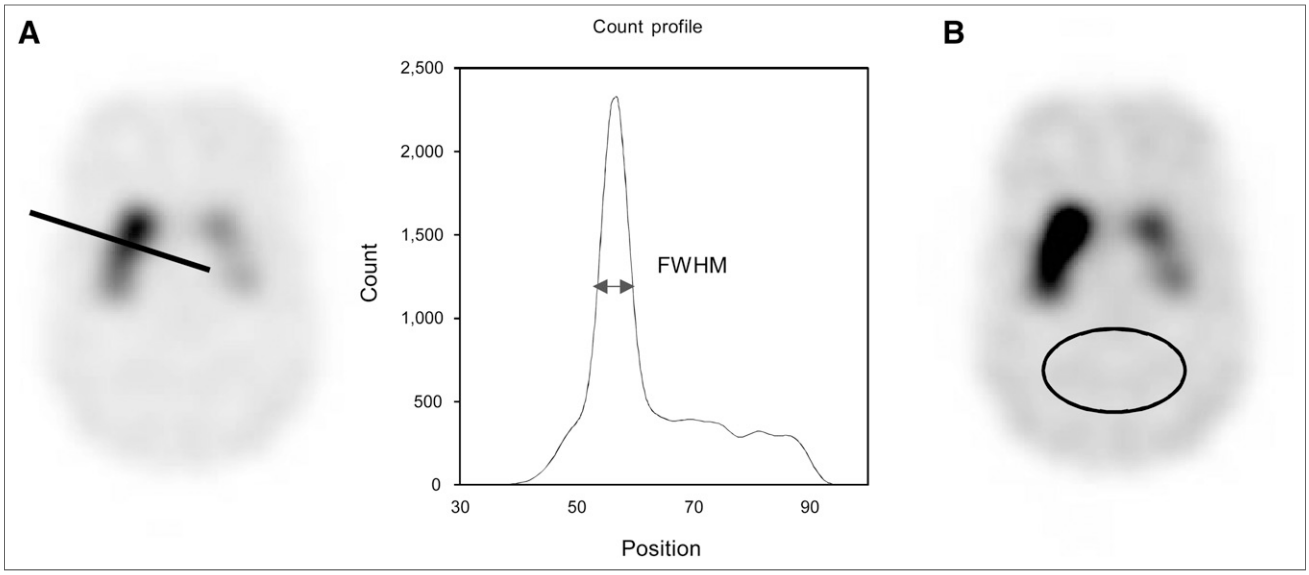

FIGURE 2. Profile and VOI setting: FWHM (A) and %CV (B).

In addition, the difference value was calculated as follows:

$$\text{Difference value} = \frac{SBR_{SS} - SBR_{CRRA}}{SBR_{SS}} \times 100(\%),$$

where SBR_{SS} is obtained using the SS mode and SBR_{CRRA} is derived from CRRA with each acquisition pattern and image process.

Statistical Analysis

The %CVs were compared using the Bonferroni/Dunn test. Differences were considered to be statistically significant at P values of less than 0.05.

RESULTS

FWHM

The FWHMs obtained by each acquisition and processing approach are shown in Figure 3. There were no clear differences between the CRRA obtained with the 2 processing approaches and the SS mode. However, with the added-reconstructed-image process, the FWHMs tended to be slightly higher in CRRA than in the SS mode (Fig. 3B).

%CV

Comparisons of the %CV with each acquisition and processing approach are shown in Figure 4. For the added-projection-data

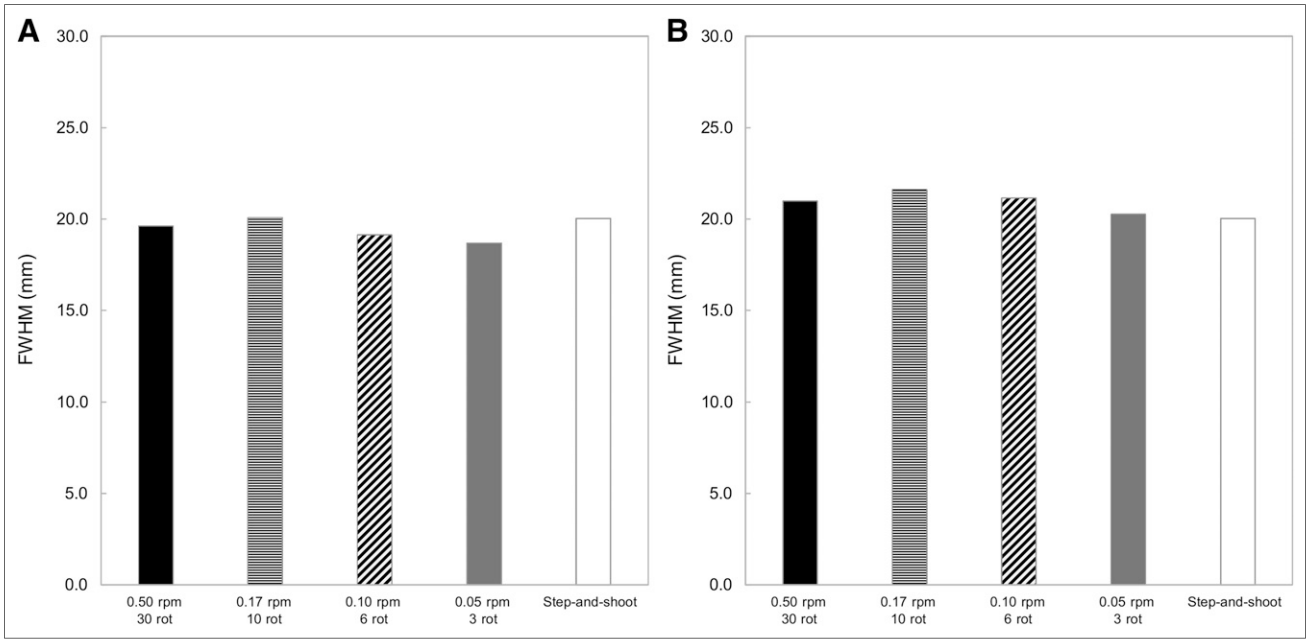

FIGURE 3. Comparison of FWHM results: added-projection-data process (A) and added-reconstructed-image process (B). Results did not clearly differ among CRRA images acquired with each rotation parameter and SS mode. rot = rotations.

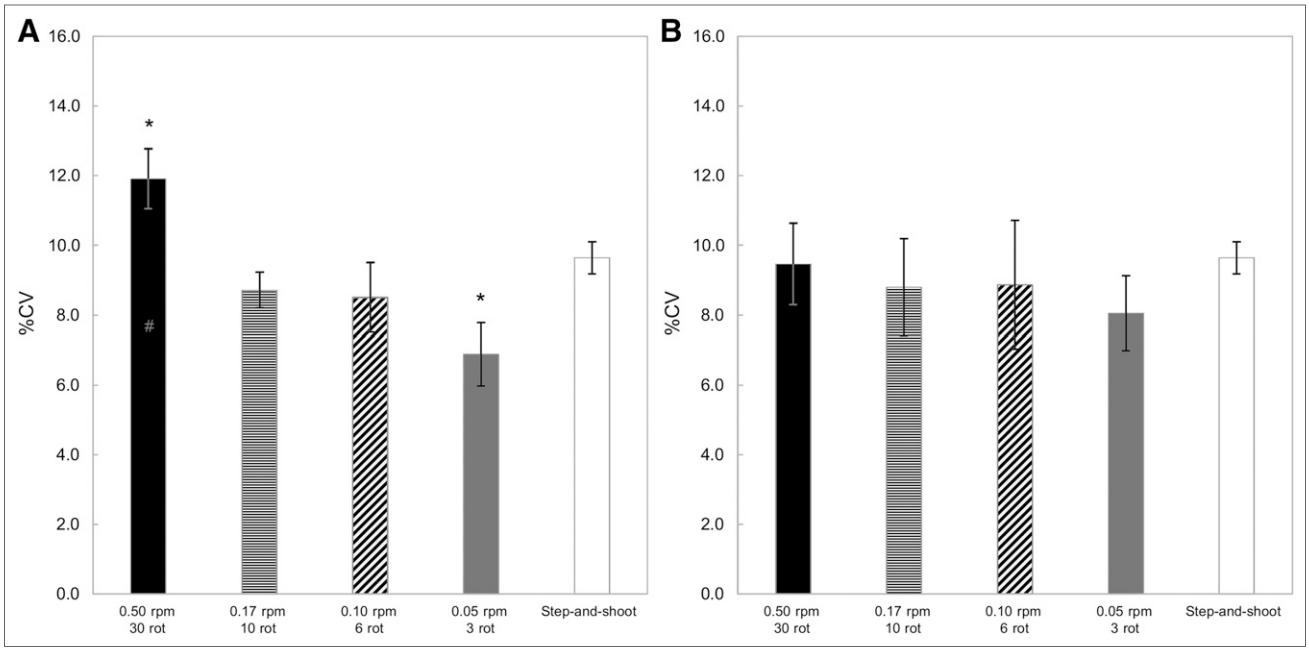

FIGURE 4. %CV: added-projection-data process (A) and added reconstruction image process (B) in which images were summed after each frame was reconstructed in independent process. %CV obtained by CRRA with added-projection-data process increased with increase in acquisition rotation speed. *$P < 0.05$ vs. SS mode and CRRA. rot = rotations.

process, although the combination of a slow rotation speed and short rotation time improved the image uniformity compared with the SS mode, the %CV obtained by CRRA increased when the rotation speed increased. With the added-reconstructed-image process, the %CVs did not significantly differ between CRRA and the SS mode. However, for the added projection data, %CV obtained with a 0.50-rpm rotation speed was significantly higher than the SS mode and other CRRA (Fig. 4A). In contrast, the %CV obtained with 0.05 rpm by 3 frames was significantly decreased compared with the SS mode. The %CVs were 11.9% ± 0.9% for 0.50 rpm by 30 frames, 8.7% ± 0.5% for 0.17 rpm by 10 frames, 8.5% ± 1.0% for 0.10 rpm by 6 frames, 6.9% ± 0.9% for 0.05 rpm by 3 frames, and 9.6% ± 0.5% for the SS mode.

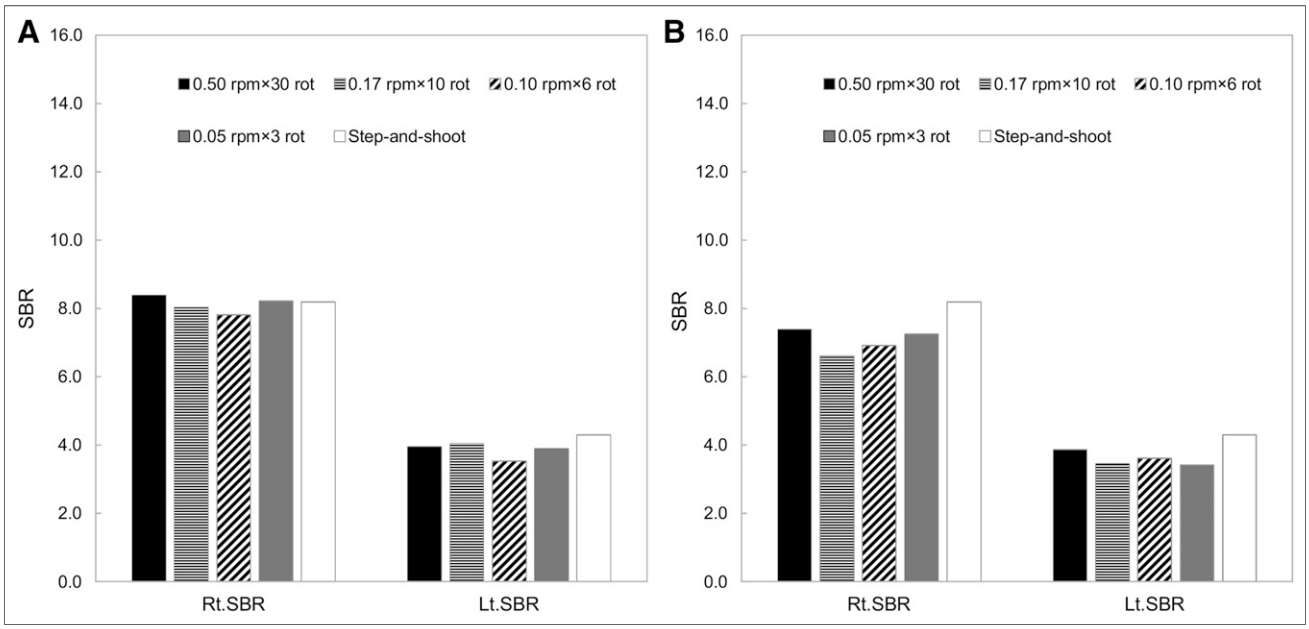

FIGURE 5. SBR comparison: added-projection-data process (A) and added-reconstructed-image process (b). SBR did not change with increase in acquisition rotation speed with added-projection-data process. However, SBR obtained by CRRA with added-reconstructed-image process was lower than that obtained with SS mode. rot = rotations.

TABLE 1
Difference Values in SBR Between CRRA and SS Mode

Difference	0.50 rpm × 30 rot	0.17 rpm × 10 rot	0.10 rpm × 6 rot	0.05 rpm × 3 rot	Mean
Between CRRA with added-projection-data process and SS mode	5.2	4.0	11.3	5.0	6.3
Between CRRA with added-reconstructed-image process and SS mode	9.9	19.5	15.8	16.1	15.3

rot = rotations.

SBR

SBRs plotted as a function of the acquisition strategies are shown in Figure 5. The SBRs obtained by CRRA with the added-projection-data process were equivalent to those obtained with the SS mode. However, the SBRs obtained with the added-reconstructed-image process were clearly decreased compared with the SS mode. The difference values in each acquisition mode are summarized in Table 1. The mean difference value between CRRA with the added-projection-data process and the SS mode was 6.3% (maximum, 11.3%; minimum, 4.0%). With the added-reconstructed-image process and the SS mode, there was a greater mean difference, at 15.3% (maximum, 19.5%; minimum, 9.9%). The SPECT images obtained by CRRA and the SS mode are shown in Figure 6. Visual assessment of the striatal detail was essentially identical for each acquisition strategy. However, the uniformity of the background area decreased with shorter acquisition times per rotation, especially when reconstructed after the addition of projection data (Fig. 6A).

DISCUSSION

CRRA as dynamic SPECT has several advantages over the SS mode in SPECT imaging. However, image noise exponentially decreases with increases in the number of counts, and as a result, for a constant injected dose and fixed level of uptake with all else being equal, noise decreases exponentially with increased acquisition time. Therefore, the acquisition parameters of CRRA affect the quality of SPECT images. In this study, we assessed the relationship between the acquisition rotation speed and the image quality of SPECT for added projection/reconstructed data. The acquisition rotation speed significantly affected SPECT image uniformity, especially when using a fast rotation speed and long rotation time.

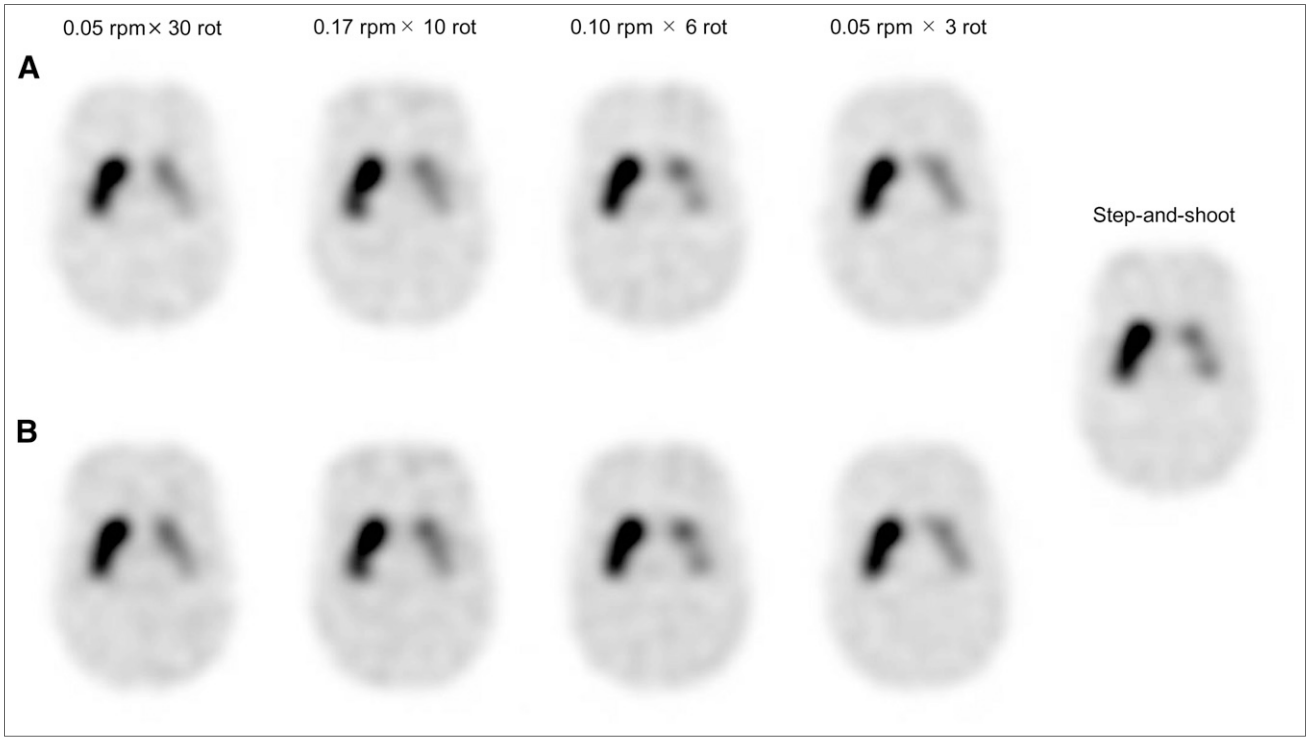

FIGURE 6. Reconstructed images of striatal phantom using CRRA and SS mode: added-projection-data process (A) and added-reconstructed-image process (B). Uniformity of background area decreased with faster rotation speed. rot = rotations.

In dopamine transporter SPECT, spatial resolution is an important factor because it can reduce underestimation of putaminal uptake due to the partial-volume effect (*14*). Our results showed that the FWHMs did not clearly differ between CRRA and the SS mode with either processing approach. Cao et al. (*15*) reported that the image quality of CRRA was similar to that of the SS mode. In addition, Kangai et al. (*16*) showed that the FWHM obtained with an optimal sampling step angle did not differ between CRRA and the SS mode. Our results agree with those of the previous studies and indicate that CRRA is appropriate for ^{123}I-FP-CIT SPECT imaging.

The %CV obtained by CRRA was superior to that obtained with the SS mode. Bieszk et al. (*17*) showed that the continuous-acquisition mode could increase the counting efficiency. For this reason, we considered that CRRA improved the image uniformity over that obtained with the SS mode. However, a combination of a fast rotation speed and increased rotation time reduced the image uniformity, especially when the projection data were added. In general, there is a trade-off between image noise and acquisition time (*18*). Because a fast rotation speed increased the image noise, the image uniformity with the added-projection-data process was significantly decreased with a fast rotation speed and an increased rotation time. Therefore, CRRA using a fast rotation speed and an increased rotation time adversely affects ^{123}I-FP-CIT SPECT imaging. In contrast, with the added-reconstructed-image process, the %CVs were not significantly different among the rotation speed and rotation time. In addition, the %CVs obtained with CRRA were equivalent to those obtained with the SS mode. The Butterworth filter plays a role in noise reduction during image reconstruction; for this reason, the %CV obtained with the added-reconstructed-image process did not affect the rotation speed or rotation time. However, we believe that it is difficult for the added-reconstructed-image process to take full advantage of the capabilities of CRRA.

The SBRs did not clearly differ between CRRA and the SS mode. However, the SBRs obtained with the added-reconstructed-image process were clearly decreased in comparison with the SS mode. According to the FWHM results, the effective spatial resolution with the added-reconstructed-image process was lower than that with the added-projection-data process. Indeed, striatal uptake is underestimated because of the limited spatial resolution of SPECT (*19*). Because spatial resolution is a key factor for improving quantitative accuracy (*20*), we suggest that the added-projection-data process be performed for CRRA to improve image quality in ^{123}I-FP-CIT SPECT.

CRRA can exclude acquisition frames with significant patient motion from the image reconstruction process. From this point of view, the most appropriate acquisition parameter of CRRA is a fast rotation speed and increased rotation time. However, we found that CRRA with a fast rotation speed was associated with lower ^{123}I-FP-CIT SPECT image quality. Therefore, for good clinical practice, it is important to minimize the risk of motion while ensuring patient comfort. If SPECT acquisition is performed using CRRA, we recommend a 0.10- to 0.17-rpm rotation speed, considering image quality and quantification and the ability to account for patient motion.

There are several limitations associated with this study. We examined only one of the commercially available SPECT/CT devices and collimators. In particular, low-energy collimators affect the quantitation of ^{123}I-FP-CIT images because of increased septal penetration of the high-energy-emission ^{123}I (*21*). Further studies are needed using several SPECT/CT scanners and collimators designed specifically for ^{123}I SPECT. A low update number depending on manufacturer recommendations was used because the aim was simply to evaluate the effect of the rotation speed and the rotation time. However, 60–80 or more updates are needed to approach convergence for small objects (*22*). Further examinations are needed to clarify this question. In addition, this study involved only phantom research, and our results might hold best when the distribution of radioactivity is relatively fixed. Image acquisition protocols should be evaluated in at least one healthy subject and one patient. Therefore, it is necessary to evaluate the effect of CRRA in clinical examinations.

CONCLUSION

We found that a combination of rotation speed and rotation times affects the image quality of ^{123}I-FP-CIT SPECT using CRRA. Our results show CRRA to outperform SS mode if the rotation speed is at least 0.17 rpm and each frame is reconstructed independently before summing. If CRRA is used for ^{123}I-FP-CIT SPECT, to take full advantage of CRRA it is necessary to use added-projection-data processes and a proper rotation speed.

DISCLOSURE

No potential conflict of interest relevant to this article was reported.

REFERENCES

1. Booij J, Speelman JD, Horstink MW, Wolters EC. The clinical benefit of imaging striatal dopamine transporters with [^{123}I] FP-CIT SPET in differentiating patients with presynaptic parkinsonism from those with other forms of parkinsonism. *Eur J Nucl Med.* 2001;28:266–272.
2. Catafau AM, Tolosa E. Impact of dopamine transporter SPECT using ^{123}I-ioflupane on diagnosis and management of patients with clinically uncertain Parkinsonian syndromes. *Mov Disord.* 2004;19:1175–1182.
3. Benamer TS, Patterson J, Grosset DG, et al. Accurate differentiation of parkinsonism and essential tremor using visual assessment of [^{123}I]-FP-CIT SPECT imaging: the [^{123}I]-FP-CIT study group. *Mov Disord.* 2000;15:503–510.
4. Covington MF, Sherman S, Lewis D, Lei H, Krupinski E, Kuo PH. Patient survey on satisfaction and impact of ^{123}I-ioflupane dopamine transporter imaging. *PLoS One.* 2015;10:e0134457.
5. Schwarz J, Linke R, Kerner M, et al. Striatal dopamine transporter binding assessed by [I-123] IPT and single photon emission computed tomography in patients with early Parkinson's disease: implications for a preclinical diagnosis. *Arch Neurol.* 2000;57:205–208.
6. Mirpour S, Turkbey EB, Marashdeh W, El Khouli R, Subramaniam RM. Impact of DAT-SPECT on management of patients suspected of parkinsonism. *Clin Nucl Med.* 2018;43:710–714.
7. Darcourt J, Booij J, Tatsch K, et al. EANM procedure guidelines for brain neurotransmission SPECT using ^{123}I-labelled dopamine transporter ligands, version 2. *Eur J Nucl Med Mol Imaging.* 2010;37:443–450.

8. Djang DS, Janssen MJ, Bohnen N, et al. SNM practice guideline for dopamine transporter imaging with ^{123}I-ioflupane SPECT 1.0. *J Nucl Med.* 2012;53:154–163.
9. QIBA profile: quantifying dopamine transporters with 123-iodine labeled ioflupane in neurodegenerative disease profile. Quantitative Imaging Biomarkers Alliance website. http://qibawiki.rsna.org/index.php/SPECT_Biomarker_Ctte. Published October 28, 2016. Last updated August 28, 2017. Accessed August 13, 2019.
10. Nakajima K, Shuke N, Taki J, et al. A simulation of dynamic SPECT using radiopharmaceuticals with rapid clearance. *J Nucl Med.* 1992;33:1200–1206.
11. Suga K, Nishigauchi K, Kume N, et al. Dynamic pulmonary SPECT of xenon-133 gas washout. *J Nucl Med.* 1996;37:807–814.
12. Suga K, Hara A, Matsumoto T, Matsunaga N. Intralobar bronchopulmonary sequestration: dynamic xenon-133 SPECT evidence of air trapping. *Br J Radiol.* 2001;74:657–661.
13. Tossici-Bolt L, Hoffmann SM, Kemp PM, Mehta RL, Fleming JS. Quantification of [^{123}I] FP-CIT SPECT brain images: an accurate technique for measurement of the specific binding ratio. *Eur J Nucl Med Mol Imaging.* 2006;33:1491–1499.
14. Soret M, Koulibaly PM, Darcourt J, Buvat I. Partial volume effect correction in SPECT for striatal uptake measurements in patients with neurodegenerative disease: impact upon patient classification. *Eur J Nucl Med Mol Imaging.* 2006;33:1062–1072.
15. Cao Z, Maunoury C, Chen CC, Holder LE. Comparison of continuous step-and-shoot versus step-and-shoot acquisition SPECT. *J Nucl Med.* 1996;37:2037–2040.
16. Kangai Y, Nagaki A, Matsutomo N, et al. Basic evaluation of sampling step angle and spatial resolution in continuous rotating acquisition with SPECT. *Nihon Hoshasen Gijutsu Gakkai Zasshi.* 2011;67:221–228.
17. Bieszk JA, Hawman EG. Evaluation of SPECT angular sampling effects: continuous versus step-and-shoot acquisition. *J Nucl Med.* 1987;28:1308–1314.
18. Magdy MK. *Basic Sciences of Nuclear Medicine*. New York, NY: Springer; 2010: 293.
19. Jaszczak JR, Coleman RE, Whitehead FR. Physical factors affecting quantitative measurement using camera-based single photon emission computed tomography (SPECT). *IEEE Trans Nucl Sci.* 1981;NS-28:69–80.
20. Soret M, Koulibaly PM, Darcourt J, Hapdey S, Buvat I. Quantitative accuracy of dopaminergic neurotransmission imaging with ^{123}I SPECT. *J Nucl Med.* 2003; 44:1184–1193.
21. Maebatake A, Sato M, Kagami R, et al. An anthropomorphic phantom study of brain dopamine transporter SPECT images obtained using different SPECT/CT devices and collimators. *J Nucl Med Technol.* 2015;43:41–46.
22. Dewaraja YK, Frey EC, Sgouros G, et al. MIRD pamphlet no. 23: quantitative SPECT for patient-specific 3-dimensional dosimetry in internal radionuclide therapy. *J Nucl Med.* 2012;53:1310–1325.